Explaining negative charging in amorphous Al_2O_3: The role of native defects

Oliver A. Dicks,* Jonathon Cottom, and Alexander L. Shluger
Department of Physics and Astronomy, University College London, Gower Street, London WC1E 6BT, United Kingdom

Valeri V. Afanas'ev
Department of Physics and Astronomy, University of Leuven, Celestijnenlaan 200d, 3001 Heverlee, Belgium

Amorphous aluminum oxide Al_2O_3 (a-Al_2O_3) layers grown by a variety of deposition techniques contain significant density of negative charges. In spite of several experimental and theoretical studies, the origin of these charges still remains unclear. We report the results of extensive Density Functional Theory (DFT) calculations of native defects - O and Al vacancies and interstitials, as well as H interstitial centers - in different charge states in both crystalline α-Al_2O_3 and in a-Al_2O_3. The results demonstrate that both the charging process and the energy distribution of traps responsible for negative charging of a-Al_2O_3 films[1] can be understood assuming that negatively charged O_i and V_{Al} defects are nearly compensated by the positively charged H_i, V_O and Al_i defects in as prepared samples. Following electron injection, the states of Al_i, V_O or H_i in the band gap become occupied by electrons and sample becomes negatively charged. The optical excitation energies into the oxide conduction band agree with the results of exhaustive photo-depopulation spectroscopy (EPDS) measurements[1]. This new understanding of the origin of negative charging of a-Al_2O_3 films is important in the development of nanoelectronic devices and solar cells.

I. INTRODUCTION

Reliable characterization and identification of electron traps in thin insulating films is of utmost importance for eliminating or limiting impact of these defects on the performance of electronic devices. In particular, amorphous aluminum oxide Al_2O_3 (a-Al_2O_3) layers grown using different deposition techniques are long known to contain significant density of negative charges [1–5] of still unclear origin. At the same time, understanding of electron trapping in amorphous alumina is important in the development of various nanoelectronic devices, including charge trap flash memory cells[1,5] and amorphous Indium Gallium Zinc Oxide (a-IGZO) transistors[6]. Furthermore, in some applications the presence of charge might even be desirable. For example, in silicon solar cells a-Al_2O_3 layers with a significant density of fixed negative charge are used to achieve electrostatic passivation [7–9] by introducing substantial band bending at the silicon side of the Si/a-Al_2O_3 interface. This leads to reduction of the surface recombination velocity thus improving the solar cell efficiency. Formation of negative charges in alumina was suggested to be a result of electron transfer from silicon to the energetically deep oxide traps. For the latter a broad variety of models has been invoked ranging from oxygen interstitials[10] to oxygen vacancies[11] and aluminum vacancies[7]. Testing the validity of these models requires understanding of how these trapping site models can explain the thermally-activated increase of the negative charge observed when annealing a-Al_2O_3 layers on Si at temperatures below 500 °C[12]. These temperatures are insufficient for defect generation since they are well below temperature range needed for atomic rearrangements in alumina, e.g., for crystallization which starts above 800 °C[13]. The previous results[14] suggest that intrinsic network sites do not provide energetically deep (>1 eV) trapping sites for electron polarons in a-Al_2O_3. Therefore in this work we investigate whether structural network imperfections, such as native defects and hydrogen ubiquitous in these samples, can explain the dominance of negative charging.

The major challenge for atomic identification of electron trapping sites in a-Al_2O_3 concerns the absence of electron spin resonance (ESR) signals associated with these electron states. Despite several attempts to observe electrons trapped in a-Al_2O_3 using ESR, only signals stemming from the interface with silicon substrate (silicon dangling bonds at the surface of Si crystal or in the near-interface Si oxide layer) or with contaminations, mostly carbon-related, have been detected so far[7,10,15–19]. We note that crystallization of alumina as a result of high temperature annealing does not eliminate electron trapping sites suggesting that they are not caused by disorder as in a-HfO_2[20]. Moreover, experiments consistently indicate that defects in question are abundant in a-Al_2O_3 films. For example, measurements of the threshold voltage shifts in a-IGZO thin film transistors provide an estimate of the electron trap density of $1\times10^{13}/cm^2$ in a 30 nm a-Al_2O_3 'charge trapping' layer[5]. On the other hand, the analysis of electron trapping in Al_2O_3 thin films in[1] provides the trap density at various depths within the film and the position of their energy levels below the conduction band minimum (CBM) using exhaustive photo-depopulation spectroscopy (EPDS). EPDS measures the energy levels of the defects by monitoring the density of electronic charge remaining in the film after the photo-excitation of electrons into the Al_2O_3 conduction band. After significant charging of the alumina films by electron injection from silicon, EPDS measurements revealed a broad range of electron trap energy levels 2-4 eV below the CBM (see Fig. 1) with a trap areal density well above $1 \times 10^{13}/cm^2$[21]. Furthermore, as can be seen in

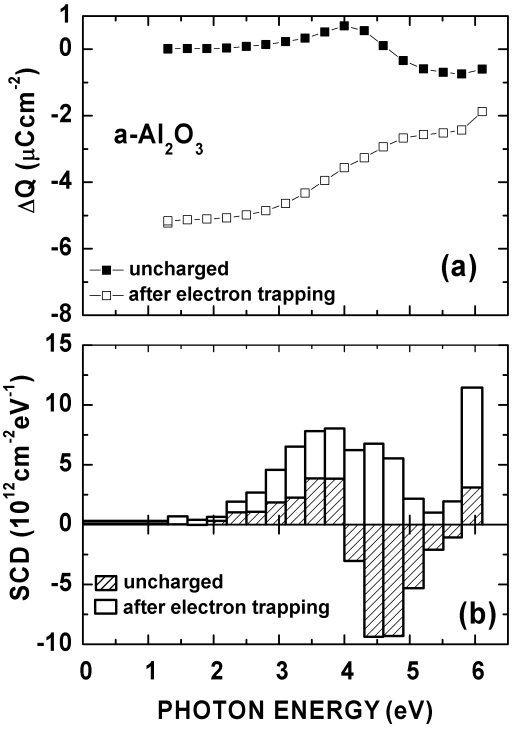

Figure 1: Oxide charge density variations induced by illumination of Si/SiO_2(4 nm)/Al_2O_3(20 nm) stacks (a) and the inferred spectral charge density diagrams (b) for uncharged and electron injected a-Al_2O_3 films.Negative SCD values correspond to the net electron trapping caused by the electron photoemission from silicon into the tunneling SiO_2 layer.The inferred energy distribution of the electron traps with respect to the CBM are shown for the as-grown (neutral) films (dashed bars) and after injecting electrons resulting in negative charging of the film (open bars).

Fig. 1, the EPDS trap spectra measured prior to the electron injection in the alumina film reveal similar energy distribution of the occupied electron states in the oxide bandgap albeit with a much lower density. This observation suggests that the fixed negative charges commonly encountered in the as-deposited alumina layers are related to the partial filling of electron traps already during Al_2O_3 film synthesis.

The EPDS measurements were confirmed by gate side trap spectroscopy when injecting electrons from silicon and sensing' (GS-TSCIS) measurements which show a peak defect density of $1.6 \times 10^{19}/\text{cm}^3$ at approximately 3.4 eV below the Al_2O_3 CBM, with a significant distribution of traps from 3.0 eV below the CBM[1]. In addition, a band of shallow traps was also identified at 1.6-1.8 eV below the CBM, with a trap density of approximately $1.6 \times 10^{19}/\text{cm}^3$ in the bulk of the Al_2O_3 films[1].

To elucidate the nature of charge trapping sites responsible for the measured energy spectrum of trapped electrons in alumina bandgap shown in Fig. 1 we performed Density Functional Theory (DFT) calculations. We assume that a-Al_2O_3 films contain native defects where the structure deviates from the stoichiometric 'pure' amorphous topology, similar to intrinsic and extrinsic defects in crystalline α-Al_2O_3 which have been widely studied computationally[22–26]. We compare the structural and electronic properties of interstitial hydrogen (H_i), oxygen vacancies (V_O), oxygen interstitials (O_i), aluminum vacancies (V_{Al}) and aluminum interstitials (Al_i) in a-Al_2O_3 and α-Al_2O_3. The calculated charge transition levels and Kohn-Sham (KS) energy levels of the defects are compared to experimental values[1] to enable identification of the defects responsible for the negative charging of a-Al_2O_3 films. We conclude that negative charging of a-Al_2O_3 films is caused predominantly by electron trapping by native defects – O vacancies and Al interstitial ions, as well as by H interstitials. These positively charged defects are compensated in as prepared samples by negatively charged O interstitial ions and Al vacancies. The charge balance is shifted to negative charge as a result of electron trapping which also creates the occupied states in the gap observed experimentally.

II. COMPUTATIONAL METHODOLOGY

The methods and potentials employed to model the a-Al_2O_3 systems have a significant impact on the structures produced. The systems considered during the course of this paper and characterized in a previous study[14] have been shown to be representative of the ALD films that are most relevant for the device applications. It is clear that the choice of potential has a direct impact on the structures produced[27–29], for the experimental results presented here the approach to model generation described in previously[14,27], was best able to produce models to facilitate a direct comparison. The substrate and growth conditions have a significant impact on the density of the a-Al_2O_3 films, which directly affects the structure of the films produced. As such, care is required in ensuring that the theoretical models produced are appropriate for the system of study.

A range of defects in a-Al_2O_3 were investigated using 10 amorphous structures generated using molecular dynamics and a melt-quench method, described previously[14]. These calculations were performed using the LAMMPS code[30], 360 atom cells, and a Born-Mayer type inter-atomic potential that had been previously used to generate a-Al_2O_3[28,31]. Briefly, the melt-quench procedure works as follows. The 360 atom cells of α-Al_2O_3 used as the initial structure were equilibrated at 300K for 10 ps, and then heated to 5000K over 20 ps and equilibrated in the melt. The structures were then cooled to 1K at a cooling rate of 10Kps^{-1}. The NPT ensemble was used with a time step of 0.1 fs. The cells were then relaxed using DFT. This method produced a-

Al_2O_3 structures with an average density of 3.14 gcm^{-3}, in agreement with experimental measurements of 2.97-3.20 gcm^{-3}[36,32,33]. As discussed in detail in [14], the obtained structural properties agree well with the experimentally measured distribution of coordination numbers[34] and radial distribution functions from x-ray and neutron diffraction studies[27]. In particular, 53%, of Al atoms are 4-coordinated by O atoms, whereas 37% and 10% are 5- and 6-coordinated, respectively. This shows that in amorphous films most Al atoms are undercoordinated with respect to α-Al_2O_3, where all Al atoms are 6-coordinated with O.

The calculations of the electronic structure were performed using the CP2K package[35]. The PBE0-TC-LRC[36] functional was used with a cutoff radius of 3.0 Å, tuned to minimize deviation from straight line error and to ensure that Koopmans' condition is obeyed (as described in[14]) similar to the implementation in[37,38]. The DZVP-MOLOPT-SR-GTH[39] basis sets were used for O, Al and H with the Goedecker-Teter-Hutter (GTH) pseudopotentials[40,41], and the auxiliary density matrix method[36] (ADMM) was used to speed up the calculations. The plane wave energy cutoff was set to 500 Ry and the SCF convergence criterion was 10^-6 a.u.. The Kohn-Sham (K-S) single-electron band gap was calculated to be 8.6 eV, which is close to the experimental optical band gap of 8.7 eV.

We note that there is a marked shift in the measured band gap between the crystalline and the amorphous phases, with α-Al_2O_3 having a band gap of 8.7 eV while the range of band gaps observed for a-Al_2O_3 are 6.0 eV - 7.0 eV, this represents a significant reduction of 20 - 30 %. This phenomenon and its relationship to the film density, structure, and dielectric properties have been examined from a theoretical viewpoint by Momida et al.[42] and experimentally by several groups using a variety of techniques.[43–47] While there is not yet a clear consensus as to the exact nature of this band gap reduction, it is clear that it is reduced significantly with respect to the crystal and the hybridization, and relative position of both the valence band and the conduction band are affected.[42,43,47,48] This last point is of critical importance when considering defects in these structures and the associated states in the band gap. Any shift in the band edges gives rise to the potential of the same defect behaving dramatically differently in the crystal and the amorphous phases. Potentially transforming a deep state in the crystal into shallow state in the amorphous film, effecting the accessible defect levels that fall within the band gap and removing some shallow states from the band gap all together. The full extent of this electronic structure, density, and motif dependence will be explored in a future publication, and as such is beyond the scope of this work.

A. Sampling defect properties in a-Al_2O-3

Defects were then created in the 360 atoms cells of both a-Al_2O_3 and α-Al_2O_3 by the addition or removal of an ion at a variety of sites, in order to sample the effect of different densities, band gaps and local atom coordination numbers. The structures were then allowed to undergo full geometry optimization using the PBE0-TC-LRC[36] hybrid functional, with a maximum force convergence criteria of 0.05 eV/Å.

In all crystals there is a finite number of non-equivalent defect sites within the primitive unit cell. It is therefore possible to calculate all configurations of a single type of defect in crystalline systems. In amorphous structures the lack of periodicity means no sites are exactly equivalent, and so any defect properties will fall within a range of values, dependent on local geometric structure and the bulk properties of the specific amorphous cell.

Different methods have been employed to sample defects in amorphous materials. One method involves sampling a variety of defect sites within a single amorphous cell[49]. This allows defect sites with different nearest neighbor configurations and bond lengths to be investigated, without having to generate a large number of amorphous geometries. However, this does mean that the range of values of the defect properties are dependent on the geometry of one cell, which may not be representative of a true amorphous material. The coordination number distribution, density, average bond length and band gap can all vary between amorphous cells, which can affect the relaxation and stable charge states of defects.

The other approach is to calculate the properties of defects in a range of different cells[50,51]. This allows a variety of local defect geometries to be sampled, which have different bond lengths and local coordination numbers, whilst also allowing for variation in bulk properties that can affect the stability of certain defect configurations and charge states. It is also less likely to be affected by anomalous cell geometries. This approach ia also applied in this work, with a single defect studied in each of the 10 different amorphous geometries that were generated. To create vacancies, atoms are removed at random, but so the distribution of the atom coordination numbers matches that of the distribution across the 10 cell geometries. Interstitial defects are created by adding an atom at a random position in the cell, with a consideration of minimum inter-atomic distances, and then performing a geometry relaxation.

This approach is still able to give a range of the defect charge transfer levels, Kohn-Sham levels and defect geometries, whilst also allowing any impact of the bulk properties to be investigated. Thus the general characteristics can be studied whilst also allowing the chance for less likely configurations to be discovered. Limited computational time means that only a finite number of configurations can be calculated, and so the properties observed are not a complete picture. However, even with 10 examples per defect, general patterns begin to emerge

and the distribution of properties observed.

B. Defect formation energies

The formation energies and charge transition levels of the defects investigated in this paper were calculated using the method described by Lany and Zunger. The chemical potential of hydrogen that is used in the calculation of the formation energies is given by the expression, $\mu_{\mathrm{H}} = E_{\mathrm{H_2}}/2$, where $\mathrm{E_{H_2}}$ is the total energy of an H_2 molecule. The chemical potential of oxygen was taken to be $\mu_{\mathrm{O}} = E_{\mathrm{O_2}}/2$, where $\mathrm{E_{O_2}}$ is the total energy of an O_2 molecule in the triplet state. Although DFT is known to over-bind the O_2 molecule leading to over estimation of the dissociation energy[52], this has not been corrected in this paper. It is known that generalized gradient approximation functionals over estimate the dissociation energy by large amounts (>1 eV)[52], but hybrid functionals, such as PBE0, better correct the self interaction error, leading to errors of approximately 0.3 eV[52]. The method used here for calculating the chemical potential of oxygen allows comparison with other papers, and, as the main properties of interest are the charge transition levels and Kohn-Sham one electron energy levels, the chemical potential will have no effect on these properties.

The aluminium chemical potential was calculated from a 256 atom cell of bulk Al in the cubic phase, after a full cell relaxation. The DFT calculation used the same PBE0-TC-LRC[36] functional and DZVP-MOLOPT-SR-GTH[39] basis sets as the other calculations in this paper.

Charge corrections to the energy, as a result of the interactions between point charges in periodic supercells[53,54] were included in the calculations of the defect formation energies. The corrections led to small shifts in the positions of the charge transfer levels by no more than 0.4 eV, due to the high dielectric constant of amorphous Al_2O_3 (9.6[55]) and the large size of the cells.

III. RESULTS OF CALCULATIONS

A. Interstitial hydrogen

Due to its presence in almost every growth environment, hydrogen is a common impurity in most metal oxides and semiconductors, including Al_2O_3[32,56,57]. Therefore it is not surprising that the negative charging observed experimentally[5,57] in a-Al_2O_3 thin films has been attributed to interstitial hydrogen (H_i). A tunneling conductivity via a mid-band gap state was observed to increase after an increase of the H content in alumina films[57]. DFT studies of H_i in crystalline Al_2O_3, using LDA[22], GGA[57] and hybrid[24–26] functionals, confirm that interstitial hydrogen has a mid-band gap energy level in alumina, close to its band offset with Si. Due to the lack of computational data on interstitial hydrogen in amorphous alumina, DFT studies of crystalline Al_2O_3 are used for comparison in this section.

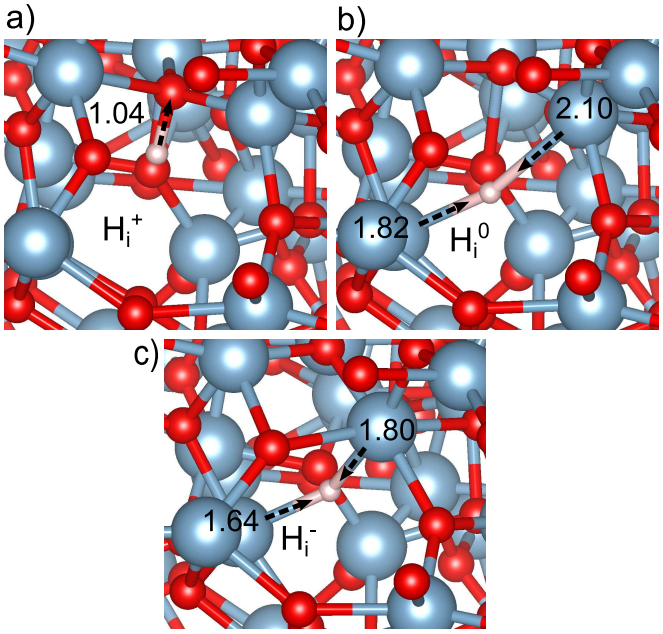

Figure 2: The structural configurations of the 3 H_i charge states, similar to those seen in crystalline Al_2O_3, with Al colored grey, O red and H white. The arrows show the direction of relaxation, with the labels showing the length of the bond. a) the H_i^+ defect which forms an OH bond. b) H_i^0 which lies between 2 Al ions as atomic hydrogen. c) H_i^- also sits between 2 Al ions, though they relax towards the negatively charged ion.

To create the defects, neutral hydrogen atoms were inserted at random positions within the 10 amorphous Al_2O_3 geometries, while ensuring initial O-H distances were greater than 1.6 Å, and then allowed to relax. This allowed the H to be positioned close to O ions with a range of coordination numbers during relaxation. After calculating the properties of the H_i^0, the different charge states were investigated by the addition or removal of an electron to the system followed by a full geometry optimization.

1. H_i^+

In crystalline alumina there are three possible charge states of interstitial hydrogen, each of which has different structural and bonding characteristics. Previous DFT calculations predict that H_i^+ forms an OH bond with a nearest neighbor oxygen in α-Al_2O_3[24–26] and θ-Al_2O_3[26], with O-H bond lengths of approximately 1.0 and 1.1 Å respectively. As can be seen in Fig 2a, the H_i^+ defect demonstrates similar behavior in a-Al_2O_3, with the proton forming an OH bond with a nearest neighbor oxygen.

The average O-H bond length over the 10 amorphous samples is 1.00 Å, with a range of 0.96-1.07 Å.

Out of the 10 H_i^+ configurations in a-Al_2O_3, 7 formed an OH bond with a 2-coordinated O ion ($^{[2]}$O), and 3 with a 3-coordinated O ($^{[3]}$O). The under-coordination of the O ions means that no Al-O bonds have to be broken to form the lowest energy configurations of the defect. This can be compared to hybrid functional calculations of α-Al_2O_3[26], where 2 of the 4 oxygen ion's Al-O bonds are broken to form the OH configuration, whilst in θ-Al_2O_3 the proton bonds with a 3-coordinated O and no O-Al bonds are broken. The H_i^+ defects in a-Al_2O_3 where the OH bond includes a $^{[2]}$O have an average formation energy that is 0.9 eV lower than those with a $^{[3]}$O. This could be due to the addition of the proton significantly lowering the energy of the localized O σ^*_{2p} type orbitals observed at the top of the valence band in bulk a-Al_2O_3, which are a direct result of the O under-coordination (refer to Jon's paper here).

2. H_i^0 and the $[H_i^+ + e_{CBM}]$ defect

The neutral hydrogen interstitial, H_i^0, behaves like an isolated hydrogen atom in crystalline Al_2O_3 and is 2 coordinated with Al[26]. It causes minimal relaxation of the surrounding lattice due to the charge neutrality[26]. The H_i^0 defect can display similar characteristics in a-Al_2O_3, where the OH bond of the H_i^+ is broken and the electron localizes on the proton, forming an isolated hydrogen atom (see Fig 2b).

However, the neutral hydrogen interstitial defect in amorphous Al_2O_3 can differ significantly from that in the crystalline material. In a-Al_2O_3 there are 2 possible configurations of the H_i^0 and, occasionally, the H_i^- defects. When an H atom or H^- ion is introduced into amorphous Al_2O_3, it is possible for it to donate its electrons into the conduction band whilst forming an OH bond with a nearest neighbor oxygen (similar to the configuration seen in Fig 2a). This can be considered as an $[H_i^+ + e_{CBM}]$ or an $[H_i^+ + 2e_{CBM}]$ defect, where e_{CBM} denotes a delocalized electron in the conduction band. DFT calculations using LDA functionals observed that for some oxides the H(+/-) charge transition level lies above the CBM[58]. This is attributed to a pinning of the H_i^0 energy level at approximately 4.5 eV below the vacuum level [58], meaning in oxides with a larger electron affinity, the energy needed to break the OH bond is greater than that required to place an electron in the conduction band.

In a review of hydrogen and muonium data[59], and their role as shallow or deep donors and acceptors, it is predicted that H_i^0 in materials with electron affinities greater than 4 eV will auto-ionize and donate an electron into the conduction band, which is confirmed by ESR data[59]. Later studies, using HSE06, demonstrate that crystalline TiO_2 and SnO_2 show similar behavior[26], both of which have electron affinities greater than 4 eV[59] and band gaps smaller than 5 eV[26]. Amorphous HfO_2 also has a $[H_i^+ + e_{CBM}]$ like defect, though the donated electron localizes at an intrinsic trap site, rather than delocalizing in the network at the conduction band minimum. This lowers its formation energy and makes this configuration energetically more favorable[50]. The trapping energy of an electron polaron in a-HfO_2 is approximately 1 eV, and so this compensates for the higher band gap of approximately 6.0 eV[50] (and a lower electron affinity of approximately 3 eV[59]).

The $[H_i^+ + e_{CBM}]$ configuration is most likely observed in a-Al_2O_3 due to the lowering of the conduction band in a-Al_2O_3 (refer to Jon's paper here) when compared to α-Al_2O_3. The lowering of the conduction band corresponds to an increase in the electron affinity towards the 4 eV suggested as the H_i^0 pinning level, and when the local structural relaxation lowers the energy surrounding the defect sufficiently, $[H_i^+ + e_{CBM}]$ can be more energetically stable than H_i^0 in the amorphous material. The $[H_i^+ + e_{CBM}]$ defect can be considered a meta-stable state in a-Al_2O_3, which is not observed in the crystalline material where the conduction band is higher, and the energy gained from structural relaxations is smaller.

3. H_i^-

In 7 out of the 10 interstitial hydrogen defects calculated, the negatively charged hydrogen interstitial forms an isolated H^- ion, as shown in Fig. 2c. This is similar to the structural geometry of the defect observed in α-Al_2O_3 and θ-Al_2O_3[26]. In the other 3 configurations an $[H_i^+ + 2e_{CBM}]$ defect is formed.

In the formation of the H_i^- defect, the electron that is introduced to the system localizes on the hydrogen, giving the ion an average Bader charge of -0.9|e|. The negative charge of the hydrogen ion causes significant relaxation of the 2 nearest neighbor Al ions, which are attracted to the interstitial hydrogen due to their formal +3 positive charge. An example of this relaxation can be seen in Fig. 2. During this relaxation the Al-H bond contracts by 0.19 to 0.36 Å, when compared to the bond lengths in the neutral charge state. Similar relaxation of the 2 nearest neighbor Al towards the H_i^- defect is observed in crystalline Al_2O_3[25,26], with the hydrogen sitting equidistant between the Al ions with a bond length of 1.67 Å. Relaxation of multiple cations towards the defect also occurs in amorphous HfO_2[50], and crystalline MgO and La_2O_3[26]. This differs from the relaxation observed in more covalent oxides, like amorphous SiO_2 [60] and crystalline SiO_2 and GeO_2[26], where the negatively charged hydrogen bonds to a single cation, causing large relaxation of the surrounding oxygens. This would suggest that the ionicity of the material strongly affects the configuration and bonding character of the H_i^- defect.

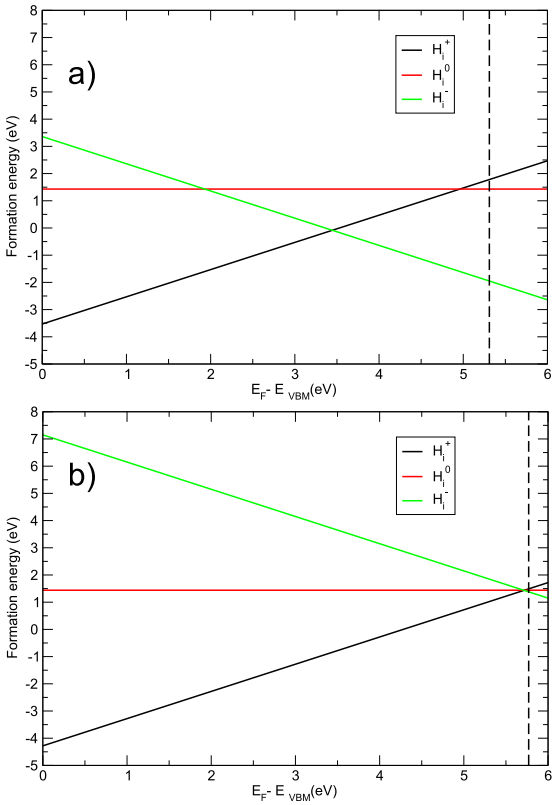

Figure 3: The formation energy of the different charge states of interstitial hydrogen against the Fermi energy with respect to the valence band. The dashed vertical line shows the position of the CBM. a) The formation energy of the H_i^+, H_i^0 and H_i^- where the OH bond is broken in the neutral and negative charge state, as seen in Fig. 2b and Fig. 2c. b) The formation energy of H_i^+, $[H_i^+ + e_{CBM}]$ and $[H_i^+ + 2e_{CBM}]$, here the (+/-) charge transfer level is at the CBM.

4. *The charge transition level and energy levels of H_i*

It is widely accepted that interstitial hydrogen in crystalline Al_2O_3 exhibits 'negative-U' behavior, meaning its +1 (H_i^+) or -1 (H_i^-) charge states are more thermodynamically stable than its neutral state (H_i^0) for all values of the Fermi energy[22,24–26]. The calculations presented here show that this holds true for interstitial hydrogen in a-Al_2O_3. As can be seen from Fig. 3, there is only a (+/-) charge transition level for the H_i^- defect, and the $[H_i^+ + 2e_{CBM}]$ defect necessarily has the charge transition level when the Fermi energy is aligned with the CBM. The formation energy of the neutral defect is never lower than that of H_i^+ or H_i^- at any value of the Fermi energy.

When only including the 7 H_i^- configurations which have a charge transition level in the band gap, the average (+/-) charge transition level lies 1.43 eV below the CBM, as can be seen in Fig. 4. The charge transition levels are shown with respect to the CBM in order to compare with experimentally measured conduction band offsets of

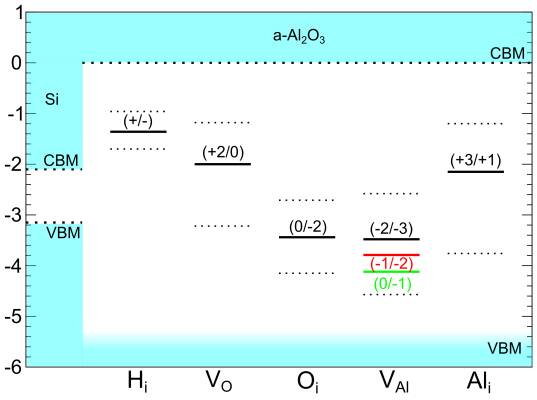

Figure 4: The average (solid line) charge transfer levels of H_i, V_O, O_i, V_{Al} and Al_i with respect to the a-Al_2O_3 CBM, with the y axis the energy in units of eV. The dashed lines represent the calculated range of the levels in the different samples. The Si/a-Al_2O_3 conduction band offset is taken from internal electron photoemission measurements[61].

a-Al_2O_3 with Si[62].

In Fig. 4 it can be seen that the (+/-) charge transition level lies above the Si conduction band, but only by an average of 0.6 eV, with the lowest (+/-) level within 0.2 eV of the Si CBM. In[1], the negative charge traps in a-Al_2O_3 are populated via the same tunneling mechanism. By varying the charging potential, traps at a range of energy levels in the alumina gap are populated when they are aligned with the injection level. Therefore H_i^- could be responsible for the negative charging observed[1]. However, the Kohn-Sham energy levels of H_i^- lie an average of 4.8 eV below the CBM, approximately 1 eV lower than the extreme range of the trap levels measured by photodepopulation spectroscopy[1]. So whilst it is possible for interstitial hydrogen to trap electrons in a-Al_2O_3[1,3,5], it is unlikely to be responsible for all the defect states observed by the EPDS measurements[1].

B. Oxygen vacancies

1. *V_O in α-Al_2O_3*

There is a large body of existing literature on oxygen vacancies in crystalline Al_2O_3, both computational[23,63,64] and experimental[65,66]. This allows calculations of V_O in α-Al_2O_3 to be used to benchmark the DFT setup and hybrid functional parameters with respect to existing studies, and to act as a point of comparison to the amorphous system.

Fig. 6 shows the formation energy of various charge states of oxygen vacancies in α-Al_2O_3. It shows that oxygen vacancies have a (+2/+1) charge transition level

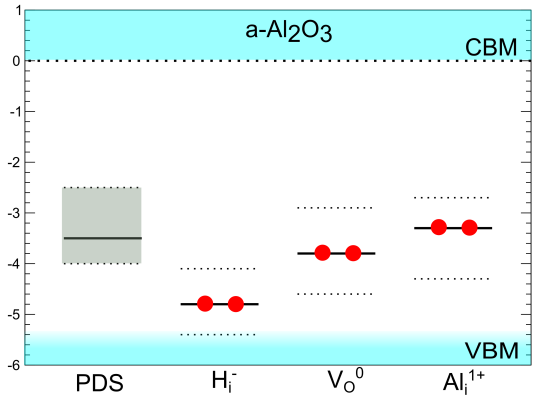

Figure 5: The average (solid black line) and range (dotted lines) of the Kohn-Sham energy levels of the Al_i, V_O or H_i defects with respect to the a-Al_2O_3 conduction band, compared to the experimental PDS trap energy level range[1]. For the PDS data the solid black line shows the energy of at the maximum density of states seen in Fig. 1.

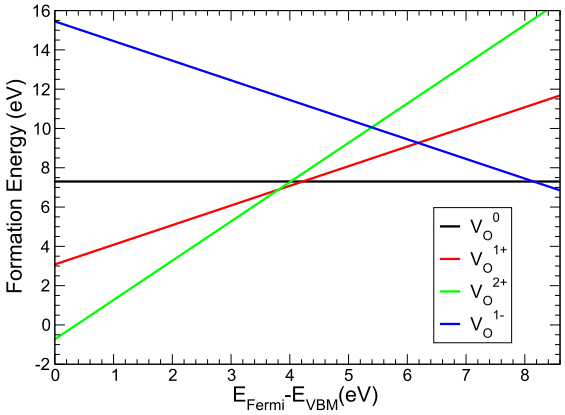

Figure 6: The formation energy of the different charge states of oxygen vacancies in α-Al_2O_3 against the Fermi energy with respect to the valence band.

at 3.8 eV above the VBM, with the (+1/0) level at 4.0 eV above the VBM, meaning that for most Fermi energies in the band gap the V_O^{2+} and V_O^0 are the most thermodynamically stable charge states of the oxygen vacancy. During the geometry relaxation of the neutrally charged oxygen vacancy, the four nearest neighbor Al move 0.01-0.10 Å towards the defect site with respect to the perfect lattice. For V_O^{2+} they relax 0.19-0.30 Å away from the vacancy site with respect to the perfect lattice. These relaxation distances are in good agreement with Choi et al.[64]. However, whilst the nearest neighbor displacements are similar, they calculate the (+2/+1) charge transition level to be 3.2 eV above the VBM, with the (+1/0) level at 4.1 eV[64]. This difference is likely due to the smaller cell size used in their paper (160 atoms), which would constrain the relaxation of the next nearest neighbor ions, increasing the energy of the V_O^{2+} defect. Over estimation of the V_O^{2+} formation energy is also observed in other calculations using smaller cell sizes[63].

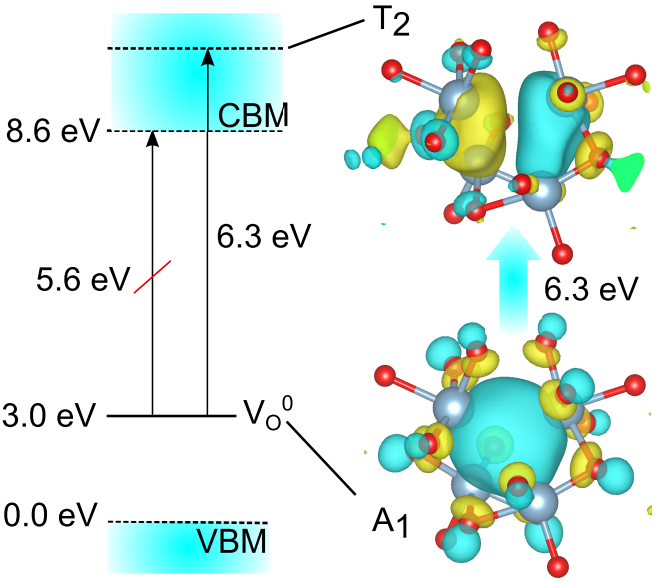

Figure 7: An energy level diagram for V_O^0 in α-Al_2O_3 showing the symmetry forbidden and allowed transitions, and the molecular orbitals of the A_1 and T_2 states involved in the symmetry allowed excitations.

Spectroscopic measurements[66] of α-Al_2O_3 assign an absorption peak at 6.4 eV to the neutral oxygen vacancy. This is greater than the 5.6 eV energy difference calculated between the V_O^0 KS energy level and the conduction band minimum. However, as oxygen in α-Al_2O_3 is four-coordinated and has tetrahedral like symmetry with point group T_d, the A_1 like character of the neutral state (see Fig. 7) has minimal wavefunction overlap with the delocalized CBM in α-Al_2O_3 as it is composed of Al 3*s* orbitals. Instead, as can be seen in Fig. 7, the defect causes a localized state in the conduction band with T_2 like character. A_1 to T_2 excitations are symmetry allowed dipole transitions and are most likely responsible for the sharp peak observed experimentally[66]. The T_2 like state (see Fig. 7) lies 6.3 eV above the neutral vacancy level, and although the energy difference between KS levels is only a first approximation for excitation energies, the calculated transition energy is in very good agreement with the experimental results.

2. *V_O in a-Al_2O_3*

Oxygen vacancies in amorphous Al_2O_3 have also been investigated using DFT methods[49,67]. However, these

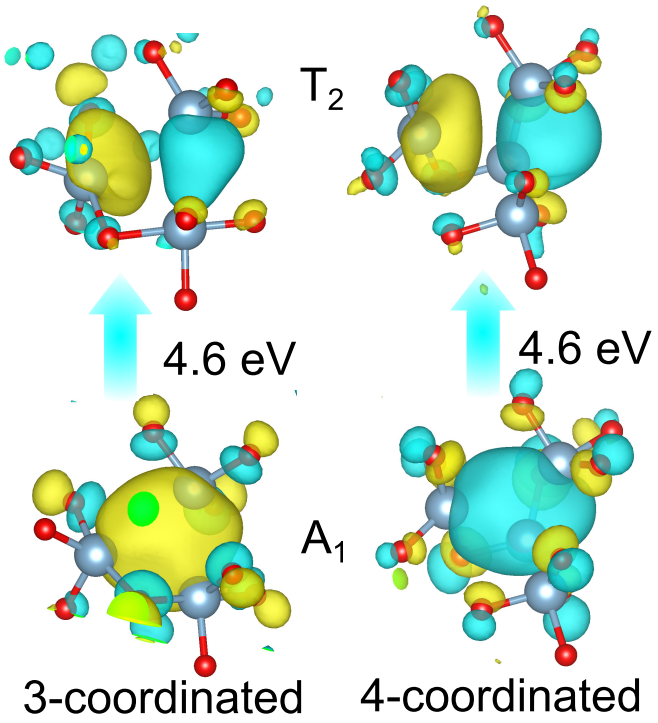

Figure 8: The molecular orbitals of the A_1 and T_2 like states of 3 and 4 coordinated V_O^0 in a-Al_2O_3, and difference in energy between their Kohn-Sham levels.

studies only model vacancies in a single cell of 80[67] and 160[49] atoms respectively, which may not capture the full range of properties of V_O. In order to improve understanding of these defects in a-Al_2O_3, the properties of oxygen vacancies at 11 defect sites in 10 geometry samples have been calculated and are presented here. The distribution of the O coordination numbers has been taken into consideration, with 7 $^{[3]}$O, 2 $^{[2]}$O and 2 $^{[4]}$O being removed in order to create the oxygen vacancies.

In amorphous Al_2O_3 only the +2 or neutral charge states of the oxygen vacancy are thermodynamically stable, as also observed by Guo et al.[49]. The (+2/0) charge transition level lies, on average, 3.5 eV above the VBM and 2.0 eV below the CBM (see Fig. 4). In the neutral charge state 2 electrons localize on the vacancy site, forming an F-center, similar to the defect in the crystalline system. As V_O^0 has a doubly occupied state in the band gap it could be responsible for the transitions seen experimentally[1], after charge injection. The high (+2/0) charge transition level suggests that before charge injection, whilst the Fermi level lies at the VBM, V_O^{2+} is the most stable configuration, which has no occupied states in the band gap. In a-Al_2O_3 there is no stable V_O^{1-} state and so it cannot be responsible for the negative charging observed in amorphous alumina films, unless it acts to compensate the negative charge of another defect.

The calculated V_O^0 KS energy levels lie on average at 4.0 eV below the CBM (see Fig. 5). The defects in the amorphous material create similar states to those observed in α-Al_2O_3. The 3- and 4-coordinated vacancy sites cause a localized state, similar to the A_1 state, to form in the band gap, and T_2 like states to appear within the conduction band (see Fig. 8). The further distortion of the tetrahedral symmetry means there is greater mixing of the states, and at 3-coordinated sites, there is significant relaxation from the next nearest neighbor Al ions, but the presence of the T_2 like state suggests there could be high oscillator strength transitions at larger excitation energies. On average the energy levels of the T_2 like states lie 4.8 eV above the energy level of V_O^0. Whilst this level lies deep into the band gap, close to the valence band in a-Al_2O_3, this is still significantly lower than the 6.5 eV excitation assigned to the neutral oxygen vacancy measured using electron energy loss spectroscopy (EELS)[68]. However, it is not clear that the excitation observed is not instead the onset of inter band transitions[68]. Due to the shift in band gap of a-Al_2O_3, the neutral vacancy will not have the same excitation energy in α and a-Al_2O_3, especially when the amorphous alumina band gap has been measured to be 6.2 eV[61].

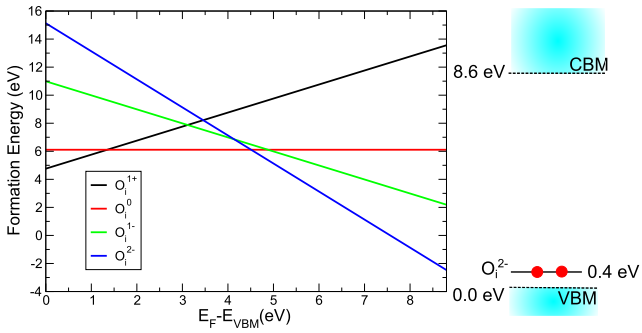

Figure 9: The formation energy of the different charge states of interstitial oxygen in α-Al_2O_3 against the Fermi energy with respect to the valence band, and the Kohn-Sham energy level position of the doubly occupied O_i^{2-} defect.

C. Interstitial oxygen

1. O_i in α-Al_2O_3

Neutrally charged oxygen interstitials in α-Al_2O_3 form an O-O dimer at the defect site, centred on the original lattice position of the O ion. In this configuration both oxygens are 3 coordinated with Al, and the O-O bond length is 1.44 Å. It has 3 thermodynamically stable charge states, as can be seen from the formation energy diagram in Fig. 9. Importantly, it traps electrons and becomes O_i^{2-} when the Fermi energy is 4.5 eV above the VBM. This is close to the 4.7 eV (0/-2) charge transition level calculated by Choi et al.[64], using the HSE06 functional.

When the oxygen interstitial captures 2 electrons to become O_i^{2-}, the O-O bond length increases to 2.15 Å. This large displacement results in both O ions becoming 4 coordinated with Al, forming tetrahedral configurations. Due to this relaxation the Kohn-Sham energy level of O_i^{2-} lies only 0.4 eV above the valence band (see Fig. 9), as both O are fully coordinated. Its role as a deep acceptor is in good agreement with previous calculations[69].

2. O_i in a-Al_2O_3

To model the oxygen interstitial in the amorphous structure, single oxygen atoms were added to the 10 different geometry samples and placed within 1.6 Å of an O ion, with 4 near [3]O, 3 near [2]O and 3 next to [4]O. Similar to the crystalline case, oxygen interstitials in a-Al_2O_3 have a deep (0/-2) charge transfer level. The average charge transfer energy lies 3.4 eV below the CBM, and 2.1 eV above the VBM. Guo et al.[49] calculate the average charge transfer level to be 2.5 eV above the VBM and similarly show there is no Fermi Energy where the O_i^- charge state is thermodynamically stable.

When the neutral charge state of the oxygen interstitial is relaxed it forms an O-O peroxy bond with the nearest neighbor oxygen. The average O-O bond length of the 10 defect configurations is 1.46 Å for the neutral charge state. When 2 electrons are added to the system, forming O_i^{2-}, the O-O bond length relaxes to an average of 2.40 Å. This large relaxation significantly lowers the energy of the defect induced σ_{2p}^* like orbitals in the conduction band, down towards the valence band. These states become occupied meaning the O_i^{2-} Kohn-Sham energy levels lie within the valence band, with no states existing in the band gap. This can be compared to the formation of hole bi-polarons in reverse[70]. In the case of bi-polaron formation, the contraction of an O-O bond to approximately 1.5 Å, after the removal of 2 electrons, pushes the now unoccupied σ_{2p}^* orbitals that form the top of the valence band into the conduction band[70].

The low lying charge transition level of interstitial oxygen means it is likely to be a source of electron trapping in a-Al_2O_3, but, the lack of states in the band gap mean it cannot explain the trap spectroscopy data[1]. Instead, it is possible that it can act as a store of negative charge which compensates for positively charged defects with unoccupied states in the gap. This could explain why experimentally the system is observed to be charge neutral before electron injection, with no transitions observed from gap states into the conduction band[1]. The transitions seen after electron injection (with the Fermi energy raised to the alumina conduction band) would then be due to the trapping of electrons in the unoccupied gap states, and the overall charging observed due to the mismatch between the number of positively and negatively charged defects[1]. Thus, whilst oxygen vacancies cannot trap negative charge in isolation, and oxygen interstitials do not have states in the gap, an oxygen Frenkel pair, for example $O_i^{2-}+V_O^0$, can have an overall negative charge and states lying in the band gap.

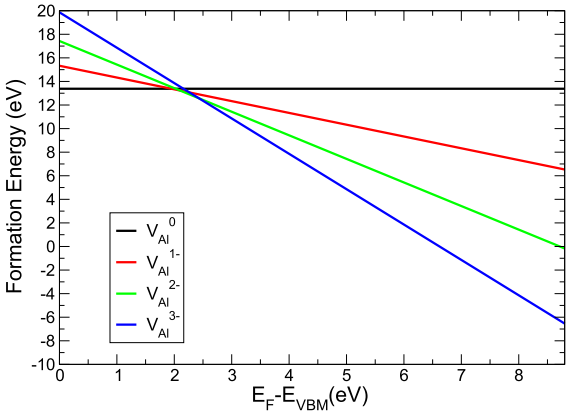

Figure 10: The formation energy of the different charge states of aluminium vacancies in α-Al_2O_3 plotted against the Fermi energy with respect to the valence band.

D. Aluminium vacancies

1. V_{Al} in α-Al_2O_3

The formation energy diagram for V_{Al} in α-Al_2O_3 (see Fig. 10) shows that the -3 charge state of the vacancy becomes stable at 2.4 eV above the VBM. This means the Al vacancy (0/-3) charge transition level lies even lower in the band gap than the interstitial oxygen (0/-2) level, and is therefore a likely source of fixed negative charge in amorphous alumina. This agrees with previous studies that show Al vacancies in α-Al_2O_3[64] and κ-Al_2O_3[23,64] are very deep acceptors, with charge transition levels close to the valence band.

The formation energies presented here are calculated using an Al chemical potential derived from DFT calculations of pure Al metal. This is equivalent to an Al-rich environment, which explains the high formation energies of the neutral vacancy, and of the charged vacancies at Fermi energies close to the valence band (see Fig. 10). However, the low formation energies at Fermi levels nearer to the conduction band suggest that it will be the dominant negatively charged defect in crystalline alumina, even in Al-rich conditions.

2. V_{Al} in a-Al_2O_3

As can be seen in Fig 4, the -3 charge state of Al vacancies in a-Al_2O_3 becomes stable when Fermi energies are on average 3.5 eV below the conduction band (2.0 eV above the valence band), which is the lowest lying charge

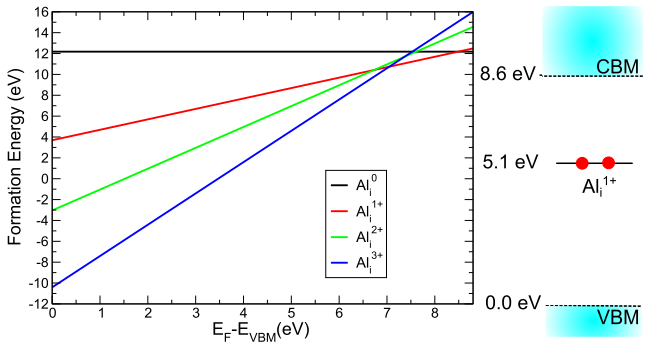

Figure 11: The formation energy of interstitial aluminium and its various charge states in α-Al_2O_3, plotted against the Fermi energy with respect to the valence band.

transition level of all the defects presented in this paper, though is very close to the O_i (0/-2) level. 10 vacancy sites were examined with 4 $^{[4]}$Al, 3 $^{[4]}$Al and 3 $^{[4]}$Al removed to create the defects. However, little dependence on coordination was observed, with a deviation in the average (-2/-3) charge transfer level of less than 0.5 eV.

It is likely that Al vacancies will acts as deep electron traps in a-Al_2O_3, but, the highest occupied Kohn-Sham energy level of V_{Al}^{3-} (across all the samples) lies 4.7 eV below the CBM, with most of the defect states lying within the valence band. This suggests that it is unlikely to be the charge trap measured by Zahid et al.[1]. It is more likely to act as a source of negative charge that compensates for positively charged defects before electron injection, similar to the mechanism described in section III C 2.

E. Interstitial aluminium

1. *Al_i in α-Al_2O_3*

On a first examination of Al interstitials in α-Al_2O_3, they do not appear to be a good candidate for the negative charging observed experimentally. The formal charge of Al in Al_2O_3 is 3+, and Bader analysis shows the system is highly ionic. Thus, the addition of an Al atom donates 3 electrons into the system without introducing any unoccupied states in the predominantly O 2*p* valence band, meaning the defect is most likely to act as a donor in α-Al_2O_3. This is demonstrated by the formation energy diagram shown in Fig. 11 where the (+3/+1) level is only 1.6 eV below the CBM. Al_i^{3+} has the lowest formation energy for a wide range of the Fermi energy, and no occupied states in the band gap available for excitations into the conduction band. There are no thermodynamically stable negative charge states of Al_i observed at any Fermi energy, to act as independent electron traps.

However, Al_i^{1+} has a doubly occupied KS energy level

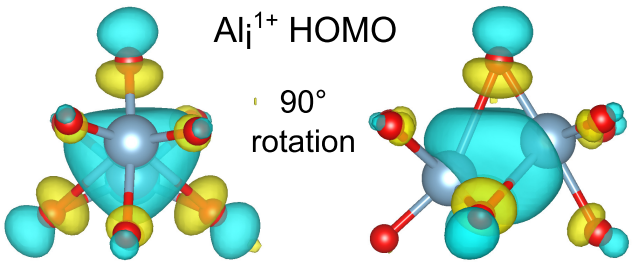

Figure 12: The iso-surface of the Al_i^{1+} HOMO, in 2 orientations so as to see the D_{3h} point symmetry. The interstitial Al and its nearest neighbor Al are both 6 coordinated with O, though some Al-O bonds are extended to 2.6 Å.

in the middle of the band gap, 3.5 eV below the CBM (see Fig. 10). The D_{3h} like point symmetry of the Al_i^{1+} highest occupied molecular orbital (HOMO), can be seen in Fig. 12. The symmetry is a result of the triangle of oxygen ions whose atomic orbitals point into the defect centre between the 2 Al ions. The electrons localize between the 2 positively charged Al ions which lowers its energy. This symmetry means that an excitation into the conduction band minimum is a dipole allowed transition (A_1 to E). Thus, at least for the crystalline system, there exists a mid gap state in the same energy range as the levels seen experimentally[1], and, unlike the oxygen vacancy, the defect state perturbs the CBM state and an occupying electron can be excited straight into the bottom of the conduction band.

2. *Al_i in a-Al_2O_3*

In a-Al_2O_3 the average KS energy level of Al_i^{1+} lies 3.4 eV below the conduction band, with a range of 2.7-4.3 eV (see Fig. 5), in very good agreement with both the PDS and GS-TSCIS measurements[1]. The average (+3/+1) charge transfer level is 2.1 eV below the CBM (see Fig. 4). This means that for a large range of the Fermi energy interstitial Al is most stable in the 3+ charge state, which has no occupied states in the gap. However, after electron injection, the unoccupied states of the Al_i^{3+} will trap electrons and become Al_i^{1+}. Al_i^{1+} has a doubly occupied state in the gap, meaning the now filled gap states can then be excited into the conduction band and electrons detected.

F. Matching the spectroscopy data

Our results suggest that O_i and V_{Al} are the dominant negatively charged defects in a-Al_2O_3. Both defects become negatively charged when the Fermi energy is approximately in the middle of the band gap, and, as can be seen in Fig. 4, their average charge transition levels lie below the Si VBM. This means that they are likely to be

in their negative charge state for most values of the Fermi energy. However, they do not have occupied levels in the band gap which could be depopulated in EPDS measurements[1]. Therefore, although they carry negative charge, they are most likely not responsible for trap states observed in[1]. On the other hand, positively charged defects, such as Al_i^{1+} and V_O^0 have occupied states in the gap with energies in the range observed in[1]. This suggests that pairs of compensating defects rather than single defects are more likely to be responsible for the behavior seen experimentally and the spectroscopic data[1].

For example, one can assume that in low density a-Al_2O_3 some Al_2O_3 molecular units are missing which implies the existence of compensating O and Al vacancies V_O^{2+} and V_{Al}^{3-}. As discussed above, V_{Al}^{3-} are unlikely to be the charge traps observed experimentally as they do not have occupied states in the right energy range. However, after trapping two extra electrons at V_O^{2+} the whole system becomes negatively charged and V_O^0 has double occupied levels at the energies corresponding to the EPDS spectra[1].

This explains why, before electron injection, no states are observed in the gap (see Fig. 1) and the charge is measured as neutral[1]. Negatively charged O_i or V_{Al} are compensated by positively charged Al_i, V_O or H_i defects, leaving the system charge nearly neutral with no states in the gap. Then, when the Fermi level is raised to the a-Al_2O_3 conduction band, electrons can occupy the Al_i, V_O or H_i states in the gap, which can then be observed spectroscopically (see Fig. 1) after excitation into the conduction band. This filling of states also leads to an overall negative charge being observed. This hypothesis is supported by measurements of electron capture cross sections that suggest that electrons trap at positively charged defect centres[2] in a-Al_2O_3, and that both positively and negatively charged defect centers are simultaneously present in the material.

To identify these traps, as a first approximation of the photo-excitation energy, the energy difference between the Kohn-Sham energy levels of the defects and the CBM, calculated using density functional theory (DFT), can be compared to the trap levels found in EPDS experiments[1,21]. Time dependent DFT (TDDFT) calculations have demonstrated that the excitation energies of transitions from localized defect states into delocalized band states in amorphous materials can be well approximated by the Kohn-Sham energy eigenvalue differences of the states[20]. In [14] it is shown that the CBM of a-Al_2O_3 is a delocalized state, and does not exhibit the electron localization seen in other oxides[71]. High electron mobilities in a-Al_2O_3 have also been measured experimentally[4]. As EPDS detects transitions by measuring charge loss due to electron drift in the alumina CB, it is important that the energy reference is taken from the mobility edge, which in a-Al_2O_3 corresponds to the CBM[4].

As was discussed in[20] the difference in Kohn-Sham energies between the defect state and the CBM can be taken as a good approximation for transition energies

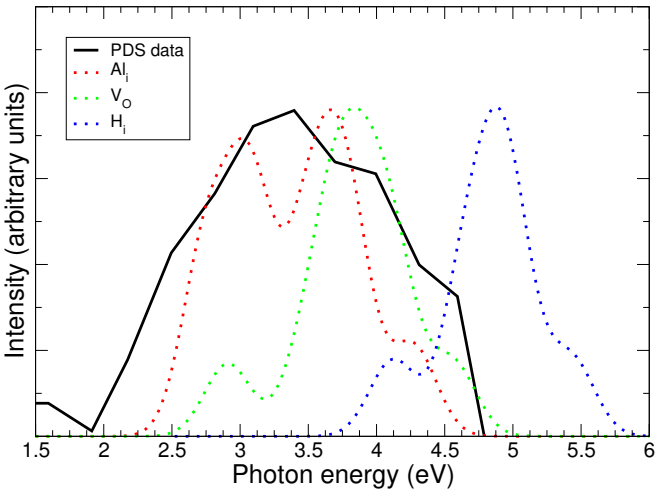

Figure 13: The transition energy spectrum of the Al_i, V_O and H_i defects, predicted using the Kohn-Sham energy level differences and broadened using Gaussians with a full width half maxima of 0.4 eV, compared to the PDS data[1] shown in Fig. 1.

calculated by TDDFT, due to the delocalized nature of the CBM[4] and the lack of localized states near the band edge[14]. With this in mind, the Kohn-Sham energy levels of Al_i, V_O or H_i, with respect to the CBM, are shown in Fig. 5, all have levels within the range measured experimentally[1]. As can be seen in Fig. 13 the distribution of energies of the Al_i and V_O match those of the EPDS measurements[1] well, but the H_i defect spectra mostly falls outside the measured spectra and so is less likely to contribute to the transitions observed. This means more than one type of 'intrinsic' defect could be responsible for the trap states, but hydrogen implantation is less likely to affect the PDS measurements. Experimental the defect species could be more confidently assigned by adjusting the growth conditions of alumina thin films so as to control the oxygen and aluminium chemical potentials.

IV. CONCLUSION

In order to understand the source of negative charging in a-Al_2O_3 films[1,3–5], the electronic properties of the defects H_i, V_O, O_i, V_{Al} and Al_i were calculated using DFT.

O_i and V_{Al} were both found to have deep acceptor levels, with the average O_i (0/-2) charge transfer level lying 3.4 eV below the a-Al_2O_3 CBM, and the average V_{Al} (-2/-3) charge transfer level lying 3.5 eV below the CBM. However, their lack of occupied energy levels in the band gap means that they are not responsible for the transitions seen in the PDS and GS-TSCIS measurements[1].

To explain spectral distribution of electron transitions observed experimentally[1] (see Fig. 1) a mechanism is proposed whereby the negatively charged O_i and V_{Al} states are compensated by the positively charged H_i, V_O

and Al_i defects. As a result of the compensation the system has nearly zero net overall charge. Following electron injection, the states of Al_i, V_O or H_i in the band gap become occupied by electrons and subsequently optical transitions into the oxide conduction band can be observed. The hypothesis regarding co-presence of oppositely charged states in the metal oxide has earlier been invoked on the basis of electron capture cross-section arguments[2]. The present study provides an atomic picture of this peculiar electrostatic condition. Furthermore, supporting the proposed interpretations, the Kohn-Sham energy levels of these defects, determined with respect to the amorphous alumina CBM (see Fig 5), overlap with the results of EPDS and GS-TSCIS measurements[1]. Finally, it is worth of noticing that the attractive Coulomb potential of the electron trapping sites would allow filling these even in the absence of externally applied electric field provided electrons have sufficient energy to tunnel to the traps. This additional electron trapping would be consistent with the observed increase of the net negative charge upon annealing of the Si/alumina structures[12]. All in one, the available experimental observations appear to be consistent with the results of our defect simulations.

V. ACKNOWLEDGMENTS

OAD acknowledges Argonne National Laboratory, USA for financial support. ALS acknowledges funding provided by EPSRC under grant EP/K01739X/1. Computer facilities on Archer service have been provided via the UKs HPC Materials Chemistry Consortium (EPSRC Grant No. EP/L000202). The authors wish to thank A.-M. El-Sayed, D. Z. Gao, J. Cottom and J. Strand for helpful discussions.

* Corresponding author. Email address: oliver.dicks.11@ucl.ac.uk

[1] M. B. Zahid, D. R. Aguado, R. Degraeve, W. C. Wang, B. Govoreanu, M. Toledano-Luque, V. V. Afanasev, and J. Van Houdt, IEEE Transactions on Electron Devices **57**, 2907 (2010), ISSN 0018-9383, URL http://ieeexplore.ieee.org/lpdocs/epic03/wrapper.htm?arnumber=5587884.

[2] V. V. Afanas'ev and A. Stesmans, Journal of Applied Physics **95**, 2518 (2004), ISSN 00218979.

[3] B. Govoreanu, D. Wellekens, L. Haspeslagh, J. De Vos, and J. Van Houdt, Technical Digest - International Electron Devices Meeting, IEDM (2006), ISSN 01631918.

[4] Y. N. Novikov, V. A. Gritsenko, and K. A. Nasyrov, Applied Physics Letters **94**, 222904 (2009), ISSN 00036951.

[5] Ya Li, Yanli Pei, Ruiqin Hu, Zimin Chen, Yiqiang Ni, Jiayong Lin, Yiting Chen, Xiaoke Zhang, Zhen Shen, Jun Liang, et al., IEEE Transactions on Electron Devices **62**, 1184 (2015), ISSN 0018-9383, URL http://ieeexplore.ieee.org/lpdocs/epic03/wrapper.htm?arnumber=7052383.

[6] K.-C. Ok, S. Oh, H.-J. Jeong, J. U. Bae, and J.-S. Park, IEEE Electron Device Letters **36**, 917 (2015), ISSN 0741-3106, URL http://ieeexplore.ieee.org/lpdocs/epic03/wrapper.htm?arnumber=7167653.

[7] G. Dingemans and W. Kessels, J. Vac. Sci. Technol. A **30**, 040802 (2012).

[8] B. Nemeth, S. P. Harvey, J. Li, D. L. Young, A. Upadhyaya, V. LaSlavia, B. G. Lee, M. R. Page, and P. Stradins, Energy Procedia **124**, 295 (2017).

[9] R. Bonilla, B. Hoex, P. Hamer, and P. Wilshaw, Phys. Stat. Solidi A **214**, 1700293 (2017).

[10] S. Kuhnhold-Pospischil, P. Saint-Cast, M. Hofmann, S. Weber, P. Jakes, R.-A. Eichel, and J. Granwehr, J. Appl. Phys. **120**, 195304 (2016).

[11] C. V. de Walle, M. Choi, J. Weber, J. Lyons, and A. Janotti, Microelectron. Eng. **102**, 211 (2013).

[12] S. Kuhnhold-Pospischil, P. Saint-Cast, A. Richter, and M. Hofmann, Appl. Phys. Lett. **109**, 061602 (2016).

[13] V. Afanas'ev, A. Stesmans, B. Mrestik, and C. Zhai, Appl. Phys.Lett **81**, 1678 (2002).

[14] O. A. Dicks and A. L. Shluger, Journal of Physics: Condensed Matter **29**, 314005 (2017), ISSN 0953-8984, URL http://stacks.iop.org/0953-8984/29/i=31/a=314005?key=crossref.5f790ab460f0691e5347d73832091481.

[15] A. Stesmans and V. Afanas'ev, J.Phys: Condens.Matter **13**, L673 (2001).

[16] A. Stesmans and V. Afanas'ev, J.Vac.Sci.Technol.B **20**, 1720 (2002).

[17] A. Stesmans and V. Afanas'ev, Appl. Phys.Lett **80**, 1957 (2002).

[18] A. Stesmans and V. Afanas'ev, Appl. Phys.Lett **85**, 3792 (2004).

[19] A. Stesmans and V. Afanas'ev, J. Appl. Phys. **97**, 033510 (2005).

[20] J. Strand, M. Kaviani, V. V. Afanas'ev, J. G. Lisoni, and A. L. Shluger, Nanotechnology **29**, 125703 (????).

[21] V. V. Afanas'ev, W. C. Wang, F. Cerbu, O. Madia, M. Houssa, and A. Stesmans, ECS Trans. **64**, 17 (2014).

[22] P. W. Peacock and J. Robertson, Applied Physics Letters **83**, 2025 (2003), ISSN 00036951.

[23] J. R. Weber, a. Janotti, and C. G. Van de Walle, Journal of Applied Physics **109**, 033715 (2011), ISSN 00218979, URL http://scitation.aip.org/content/aip/journal/jap/109/3/10.1063/1.3544310.

[24] A. M. Holder, K. D. Osborn, C. J. Lobb, and C. B. Musgrave, Physical Review Letters **111**, 065901 (2013), ISSN 00319007, 1303.6713.

[25] L. Gordon, H. Abu-Farsakh, A. Janotti, and C. G. Van de Walle, Scientific Reports **4**, 7590 (2014), ISSN 2045-2322.

[26] H. Li and J. Robertson, Journal of Applied Physics **115**, 203708 (2014), ISSN 0021-8979, URL http://aip.scitation.org/doi/10.1063/1.4878415.

[27] P. Lamparter and R. Kniep, Physica B **236**, 405 (1997).

[28] G. Gutiérrez and B. Johansson, Physical Review B **65**, 104202 (2002), ISSN 0163-1829.

[29] K. Choudhary, T. Liang, A. Chernatynskiy, S. R. Phillpot, and S. B. Sinnott, Journal of Physics: Con-

densed Matter **27**, 305004 (2015), ISSN 0953-8984, URL http://stacks.iop.org/0953-8984/27/i=30/a=305004?key=crossref.32849ee6c5eea308d8594d1f8bd14aa9.

[30] S. Plimpton, Journal of Computational Physics **117**, 1 (1995), ISSN 0021-9991.

[31] L. Bläckberg, E. Metsanurk, A. Tamm, A. Aabloo, and M. Klintenberg, Nuclear Instruments and Methods in Physics Research Section A: Accelerators, Spectrometers, Detectors and Associated Equipment **759**, 10 (2014), ISSN 01689002, URL http://linkinghub.elsevier.com/retrieve/pii/S0168900214003416.

[32] M. D. Groner, F. H. Fabreguette, J. W. Elam, and S. M. George, Chemistry of Materials **16**, 639 (2004), ISSN 08974756.

[33] B. Ilic, S. Krylov, and H. G. Craighead, Journal of Applied Physics **108**, 044317 (2010), ISSN 00218979.

[34] S. Lee, S. Park, Y. Yi, and C. Ahn, Physical Review Letters **103**, 095501 (2009), ISSN 0031-9007, URL http://link.aps.org/doi/10.1103/PhysRevLett.103.095501.

[35] J. VandeVondele, M. Krack, F. Mohamed, M. Parrinello, T. Chassaing, and J. Hutter, Computer Physics Communication **167**, 103 (2005), ISSN 0010-4655.

[36] M. Guidon, J. Hutter, and J. VandeVondele, Journal of Chemical Theory and Computation **5**, 3010 (2009), ISSN 15499618.

[37] L. Kronik, T. Stein, S. Refaely-Abramson, and R. Baer, Journal of Chemical Theory and Computation **8**, 1515 (2012), ISSN 1549-9618, URL http://pubs.acs.org/doi/abs/10.1021/ct2009363.

[38] A. Karolewski, L. Kronik, and S. Kümmel, Journal of Chemical Physics **138** (2013), ISSN 00219606.

[39] J. VandeVondele and J. Hutter, The Journal of Chemical Physics **127**, 114105 (2007), ISSN 0021-9606, URL http://www.ncbi.nlm.nih.gov/pubmed/17887826.

[40] S. Goedecker, M. Teter, and J. Hutter, Physical Review B **54**, 1703 (1996), ISSN 0163-1829, URL http://link.aps.org/doi/10.1103/PhysRevB.54.1703.

[41] C. Hartwigsen, S. Goedecker, and J. Hutter, Physical Review B **58**, 3641 (1998), ISSN 0163-1829, URL http://link.aps.org/doi/10.1103/PhysRevB.58.3641.

[42] H. Momida, T. Hamada, Y. Takagi, T. Yamamoto, T. Uda, and T. Ohno, Physical Review B **73**, 054108 (2006), ISSN 1098-0121, URL http://link.aps.org/doi/10.1103/PhysRevB.73.054108https://link.aps.org/doi/10.1103/PhysRevB.73.054108.

[43] E. O. Filatova and A. S. Konashuk, Journal of Physical Chemistry C **119**, 20755 (2015), ISSN 19327455.

[44] P. Snijders, L. Jeurgens, and W. Sloof, Surface Science **496**, 97 (2002), ISSN 0039-6028, URL http://www.sciencedirect.com/science/article/pii/S0039602801015916.

[45] V. V. Afanas'Ev, A. Stesmans, B. J. Mrstik, and C. Zhao, Applied Physics Letters **81**, 1678 (2002), ISSN 00036951.

[46] V. V. Afanas'ev, A. Stesmans, G. Brammertz, A. Delabie, S. Sionke, A. O'Mahony, I. M. Povey, M. E. Pemble, E. O'Connor, P. K. Hurley, et al., Applied Physics Letters **94**, 202110 (2009).

[47] R. Lizárraga, E. Holmström, S. C. Parker, and C. Arrouvel, Phys. Rev. B **83**, 094201 (2011), URL https://link.aps.org/doi/10.1103/PhysRevB.83.094201.

[48] D. Colleoni, G. Miceli, and A. Pasquarello, Appl. Phys. Lett. **107**, 211601 (2015), ISSN 0003-6951, URL http://dx.doi.org/10.1063/1.4936240.

[49] Z. Guo, F. Ambrosio, and A. Pasquarello, Applied Physics Letters **109**, 062903 (2016), ISSN 00036951, URL http://dx.doi.org/10.1063/1.4961125.

[50] M. Kaviani, V. V. Afanas'ev, and A. L. Shluger, Physical Review B **95**, 075117 (2017), ISSN 2469-9950, URL http://link.aps.org/doi/10.1103/PhysRevB.95.075117https://link.aps.org/doi/10.1103/PhysRevB.95.075117.

[51] A.-M. El-Sayed, M. B. Watkins, T. Grasser, V. V. Afanas'ev, and A. L. Shluger, Physical Review Letters **114**, 115503 (2015), ISSN 0031-9007, URL https://link.aps.org/doi/10.1103/PhysRevLett.114.115503.

[52] S. Klüpfel, P. Klüpfel, and H. Jónsson, The Journal of Chemical Physics **137**, 124102 (2012), ISSN 0021-9606, 1308.6527, URL http://aip.scitation.org/doi/10.1063/1.4752229.

[53] S. Lany and A. Zunger, Physical Review B **78**, 235104 (2008), ISSN 1098-0121, URL http://link.aps.org/doi/10.1103/PhysRevB.78.235104.

[54] H.-P. Komsa, T. T. Rantala, and A. Pasquarello, Physical Review B **86**, 045112 (2012), ISSN 1098-0121, URL https://link.aps.org/doi/10.1103/PhysRevB.86.045112.

[55] K. Shamala, L. Murthy, and K. Narasimha Rao, Materials Science and Engineering B **106**, 269 (2004), ISSN 09215107, URL http://linkinghub.elsevier.com/retrieve/pii/S0921510703004756.

[56] M. M. El-Aiat and F. A. Kröger, Journal of Applied Physics **53**, 3658 (1982), ISSN 00218979.

[57] D. R. Jennison, P. A. Schultz, and J. P. Sullivan, Physical Review B **69**, 041405 (2004), ISSN 1098-0121, URL http://link.aps.org/doi/10.1103/PhysRevB.69.041405.

[58] C. G. Van De Walle, Physica B: Condensed Matter **423**, 626 (2006), ISSN 09214526.

[59] S. F. J. Cox, Journal of Physics: Condensed Matter **15**, R1727 (2003), ISSN 0953-8984, URL http://stacks.iop.org/0953-8984/15/i=46/a=R01?key=crossref.466704a23bf53b7dece8b8c87df3fb96.

[60] A. M. El-Sayed, Y. Wimmer, W. Goes, T. Grasser, V. V. Afanas'Ev, and A. L. Shluger, Physical Review B **92**, 014107 (2015), ISSN 1550235X.

[61] V. V. Afanas'ev, A. Stesmans, and W. Tsai, Applied Physics Letters **82**, 245 (2003), ISSN 00036951.

[62] V. V. Afanas'Ev, M. Houssa, A. Stesmans, C. Merckling, T. Schram, and J. A. Kittl, Applied Physics Letters **99**, 072103 (2011), ISSN 00036951.

[63] D. Liu, S. Clark, and J. Robertson, Applied Physics Letters **96**, 032905 (2010), ISSN 0003-6951, URL http://dx.doi.org/10.1063/1.3293440.

[64] M. Choi, A. Janotti, and C. G. Van De Walle, Journal of Applied Physics **113**, 044501 (2013), ISSN 00218979.

[65] M. J. Springis and J. A. Valbis, Physica Status Solidi (b) **123**, 335 (1984), ISSN 03701972, URL http://doi.wiley.com/10.1002/pssb.2221230136.

[66] V. A. Pustovarov, V. S. Aliev, T. V. Perevalov, V. A. Gritsenko, and A. P. Eliseev, Journal of Experimental and Theoretical Physics **111**, 989 (2010), ISSN 1063-7761.

[67] D. Liu, Y. Guo, L. Lin, and J. Robertson, Journal of Applied Physics **114**, 083704 (2013), ISSN 00218979.

[68] T. V. Perevalov, O. E. Tereshenko, V. A. Gritsenko, V. A. Pustovarov, A. P. Yelisseyev, C. Park, J. H. Han, and C. Lee, Journal of Applied Physics **108**, 013501 (2010), ISSN 00218979.

[69] L. R. C. Fonseca, D. Liu, and J. Robertson, Applied Physics Letters **93**, 122905 (2008), ISSN 0003-6951, URL http://aip.scitation.org/doi/10.1063/1.2991287.

[70] J. Strand, O. A. Dicks, M. Kaviani, and A. L. Shluger, Microelectronic Engineering **178**, 235 (2017), ISSN 01679317, URL http://linkinghub.elsevier.com/retrieve/pii/S0167931717302095.

[71] M. Kaviani, J. Strand, V. V. Afanas'Ev, and A. L. Shluger, Physical Review B **94**, 020103 (2016), ISSN 1550235X.